

N-type core-shell heterostructured Bi_2S_3@Bi nanorods/polyaniline hybrids for stretchable thermoelectric generator

Lu Yang(杨璐), Chenghao Liu(刘程浩), Yalong Wang(王亚龙), Pengcheng Zhu(朱鹏程),Yao Wang(王瑶), and Yuan Deng(邓元)

Citation: Chin. Phys. B, 2022, 31 (**2**): 028204. DOI: 10.1088/1674-1056/ac272e
Journal homepage: http://cpb.iphy.ac.cn; http://iopscience.iop.org/cpb

What follows is a list of articles you may be interested in

The n-type Si-based materials applied on the front surface of IBC-SHJ solar cells

Jianhui Bao(包建辉), Ke Tao(陶科), Yiren Lin(林苡任), Rui Jia(贾锐), Aimin Liu(刘爱民)
Chin. Phys. B, 2019, 28 (**9**): 098201. DOI: 10.1088/1674-1056/ab33ec

Imaging the diffusion pathway of Al^{3+} ion in NASICON-type $(Al_{0.2}Zr_{0.8})_{20/19}Nb(PO_4)_3$ as electrolyte for rechargeable solid-state Al batteries

Jie Wang(王捷), Chun-Wen Sun(孙春文), Yu-Dong Gong(巩玉栋), Huai-Ruo Zhang(张怀若), Jose Antonio Alonso, María Teresa Fernández-Díaz, Zhong-Lin Wang(王中林), John B Goodenough
Chin. Phys. B, 2018, 27 (**12**): 128201. DOI: 10.1088/1674-1056/27/12/128201

Performance of n-type silicon/silver composite anode material in lithium ion batteries: A study on effect of work function matching degree

Guo-Jun Xu(徐国军), Chen-Xin Jin(金晨鑫), Kai-Jie Kong(孔凯捷), Xi-Xi Yang(杨西西), Zhi-Hao Yue(岳之浩), Xiao-Min Li(李晓敏), Fu-Gen Sun(孙福根), Hai-Bin Huang(黄海宾), Lang Zhou(周浪)
Chin. Phys. B, 2018, 27 (**10**): 108201. DOI: 10.1088/1674-1056/27/10/108201

Highly sensitive polymer photodetectors with a wide spectral response range

Mile Gao(高米勒), Wenbin Wang(王文斌), Lingliang Li(李凌亮), Jianli Miao(苗建利), Fujun Zhang(张福俊)
Chin. Phys. B, 2017, 26 (**1**): 018201. DOI: 10.1088/1674-1056/26/1/018201

In-situ characterization of electrochromism based on ITO/PEDOT:PSS towards preparation of high performance device

Xue-Jin Wang(王学进), Zheng-Fei Guo(郭正飞), Jing-Yu Qu(曲婧毓),Kun Pan(潘坤), Zheng Qi(祁铮), Hong Li(李泓)
Chin. Phys. B, 2016, 25 (**2**): 028201. DOI: 10.1088/1674-1056/25/2/028201

SPECIAL TOPIC — Organic and hybrid thermoelectrics

N-type core-shell heterostructured Bi_2S_3@Bi nanorods/polyaniline hybrids for stretchable thermoelectric generator

Lu Yang(杨璐)[1,†], Chenghao Liu(刘程浩)[1,†], Yalong Wang(王亚龙)[1], Pengcheng Zhu(朱鹏程)[4], Yao Wang(王瑶)[1,3,‡], and Yuan Deng(邓元)[2,3,§]

[1] *School of Materials Science and Engineering, Beihang University, Beijing* 100191, *China*
[2] *Hangzhou Innovation Institute, Beihang University, Hangzhou* 310052, *China*
[3] *Research Institute for Frontier Science, Beihang University, Beijing* 100191, *China*
[4] *School of Physics and Microelectronics, Zhengzhou University, Zhengzhou* 450001, *China*

(Received 18 August 2021; revised manuscript received 9 September 2021; accepted manuscript online 16 September 2021)

With the growing need on distributed power supply for portable electronics, energy harvesting from environment becomes a promising solution. Organic thermoelectric (TE) materials have advantages in intrinsic flexibility and low thermal conductivity, thus hold great prospect in applications as a flexible power generator from dissipated heat. Nevertheless, the weak electrical transport behaviors of organic TE materials have severely impeded their development. Moreover, compared with p-type organic TE materials, stable and high-performance n-type counterparts are more difficult to obtain. Here, we developed a n-type polyaniline-based hybrid with core-shell heterostructured Bi_2S_3@Bi nanorods as fillers, showing a Seebeck coefficient −159.4 μV/K at room temperature. Further, a couple of n/p legs from the PANI-based hybrids were integrated into an elastomer substrate forming a stretchable thermoelectric generator (TEG), whose function to output stable voltages responding to temperature differences has been demonstrated. The *in situ* output performance of the TEG under stretching could withstand up to 75% elongation, and stability test showed little degradation over a one-month period in the air. This study provides a promising strategy to develop stable and high thermopower organic TEGs harvesting heat from environment as long-term power supply.

Keywords: polyaniline-based hybrids, thermoelectric properties, n-type, stretchable electronics

PACS: 82.35.Cd, 84.60.Rb, 84.60.Bk, 85.80.Fi **DOI:** 10.1088/1674-1056/ac272e

1. Introduction

Rapid development of flexible electronics brings a new era of technologically immersive world, and an everincreasing need for portable, distributed and long-term power source has thus been raised. Thermoelectric (TE) materials can realize direct energy conversion between thermal energy and electricity, thus provide a promising solution to harvest heat energy from environment for power generation. The performances of TE materials are evaluated via figure of merit $ZT = \sigma S^2/\kappa$, where σ is electrical conductivity, S is Seebeck coefficient, and κ is thermal conductivity. Organic thermoelectric materials, such as conducting polymers,[1–4] organic semiconductors,[5,6] organic/inorganic hybrids[7–11] have emerged recently as successful candidates. Despite their relatively low electrical transport properties compared with the inorganic counterparts, they have significant advantages in easy processing and low cost; moreover, recent progress has shown a catching up trend in both materials properties and device performances.[12–15]

Nevertheless, the scarcity of high-performance of n-type flexible TE materials is still a big challenge due to the less-efficient hopping transport mechanism and low electron affinity caused chemical instability, which has significantly impeded the development of flexible thermoelectric generators (TEGs) assembled from matched p/n pairs of TE legs. Several studies show that the organic/inorganic hybrids are of particular potential to realize high-performance n-type TE materials. For instance, via incorporating n-type inorganic fillers into polymer matrix, Wan *et al.* reported a high power factor ($PF = \sigma S^2$) of 0.45 mW/m·K^2 and ZT of 0.28 at 373 K for a hybrid superlattice of alternating inorganic TiS_2 monolayers and organic cations.[6] Cai *et al.* designed n-type Ag_2Se/Ag/CuAgSe thermoelectric composite film supported by a porous nylon membrane presenting an ultrahigh power factor of 2231.5 μW/m·K^2 at 300 K.[13] In practice, when flexible TEGs applied as wearable electronics, these devices generally suffer nonuniform strain, thus mechanical compliance and stability are highly required. The TEGs assembled from organic TE materials are generally flexible, yet their stretchability has been addressed to less extent.

Based on our previous studies, a heat treatment strategy is effective in transforming p-type polyaniline (PANI)-based hybrids into n-type, where after high temperature treatment, the concentration of the major hole carrier from p-type PANI quickly falls, and the electrons from n-type Bi_2S_3 gradually

[†]These authors contributed equally.
[‡]Corresponding author. E-mail: wang-yao@buaa.edu.cn
[§]Corresponding author. E-mail: dengyuan@buaa.edu.cn

© 2022 Chinese Physical Society and IOP Publishing Ltd

dominate the hybrid film.[16] Due to intrinsically weak electrical transport behaviors of Bi_2S_3,[17] the power factor of the n-type Bi_2S_3/PANI is still magnitude lower than that of PANI-based p-type hybrids. Herein, core-shell heterostructured Bi_2S_3@Bi nanorods were constructed to increase the electrical conductivity of fillers via introducing a high conductivity Bi coating layer. The same heat treatment strategy has been employed to transform p-type PANI-based hybrids into stable n-type at room temperature. Further, a stretchable TEG has been integrated from n-type Bi_2S_3@Bi/PANI and p-type Te-MWCNT/PANI hybrids with elastomer substrate, and the function as power generator has been demonstrated.

2. Experimental details

2.1. Materials

Bismuth chloride ($BiCl_3$) and hydrazine hydrate (N_2H_4) were supplied by Shanghai Macklin Biochemical Co., Ltd., China. Sodium sulfide nonahydrate ($Na_2S{\cdot}9H_2O$) with purity higher than 98.0% was purchased from Xilong Chemical Reagent Co. Ltd., China. All the raw chemicals, including ethylene glycol, C_6H_7N, HCl, $(NH)_2S_2O_8$, LiCl, NaOH, m-cresol, and camphorsulfonic acid were used as received without further purification.

2.2. Fabrication of Bi_2S_3@Bi nanorods

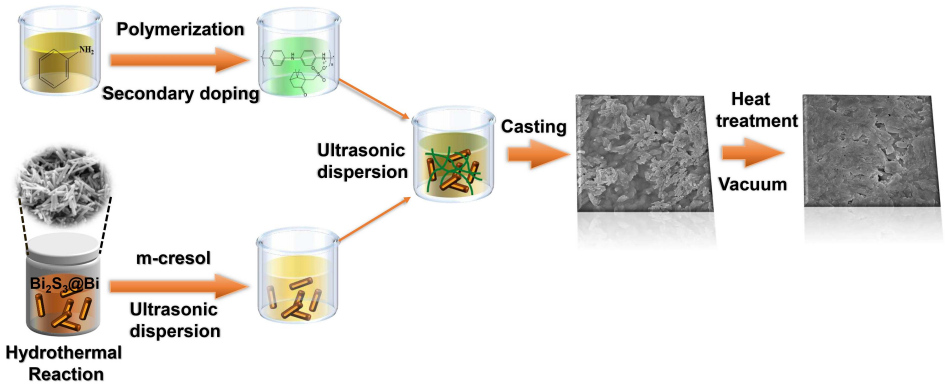
The synthesis of Bi_2S_3@Bi core-shell structure is based on an *in situ* reduction reaction that Bi element could be reduced from Bi_2S_3 by a strong reductant in alkaline solution. Thus, the surface of Bi_2S_3 nanorod would transform to Bi via controlling the reaction time. Here, the following reaction was employed:[18]

$$Bi_2S_3 + NH_2NH_2 \rightarrow Bi + N_2 + H_2S. \quad (1)$$

Here 5.7 g $BiCl_3$ was added to 24 ml distilled water with stirring, and then 6 ml HCl (36 wt%) was added dropwise until the white precipitate (BiOCl) was dissolved completely. 10.5 g $Na_2S{\cdot}9H_2O$ was dissolved in 15 ml deionized water completely. The solutions were then mixed and stirred for 30 min. Next, the mixed solution was transferred to a teflon-lined autoclave and maintained at 180 °C for 12 h. After the reaction, the product was washed with deionized water and alcohol and dried in an oven at 353 K to obtain clean Bi_2S_3 nanorods. Afterwards, 1 g NaOH was added to 100 ml distilled water with stirring, and 10 ml of N_2H_4 dropped at a constant speed was added. 1 g Bi_2S_3 nanorods were added into the solution and stirred for 30 min forming a brown-black suspension. After ultrasonic dispersing the suspension for 20 min, it was transferred to a teflon-lined autoclave and was maintained at 180 °C for 1 h, 2 h and 3 h, respectively. After the reaction, the product was washed with deionized water and alcohol and dried in an oven at 80 °C.

2.3. Fabrication of Bi_2S_3@Bi/PANI hybrid films

The processing has been carried out according to our previous study on PANI-based hybrid films[19] and n-type Bi_2S_3/PANI.[16] The procedures are illustrated in Scheme 1. The as-prepared Bi_2S_3@Bi nanorods with different weight fractions from 50 wt% to 90 wt% were first ultrasonically dispersed in m-cresol, and then mixed with PANI solution ultrasonically. The obtained Bi_2S_3@Bi /PANI solution was cast on glass substrates and dried at 60 °C to form a dense film. After the films were completely dried, they were rapidly heat treated at 210 °C in vacuum for 10 min, followed by cooling to room temperature.

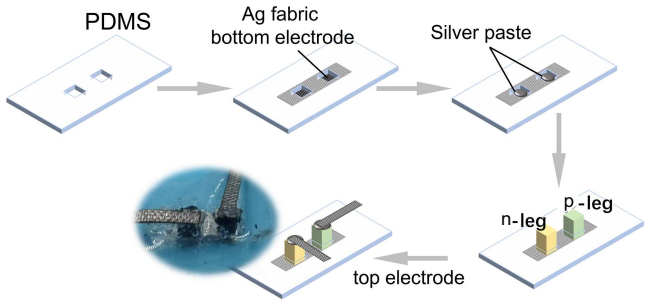


Scheme 1. Schematic illustration on the processing procedures of n-type Bi_2S_3@Bi/PANI hybrid films.

2.4. Integration of n/p polyaniline-based hybrids to stretchable TEG

The p-type TE material used here is TeMWCNT/PANI hybrid film with Te nanorod around 60 wt% and MWCNT around 10 wt%, with TE parameters of $S = 40 \pm 3$ μV/K, $\sigma =$ 196 S/cm based on our previous work.[20] The PANI-based hybrid films were first hot-pressed at 160 °C and 0.35 MPa to form TE legs with size 1 mm × 1 mm × 1.3 mm. The illustration on a pair of p/n TEG integration flow is shown in Scheme 2. PDMS was employed as elastomer substrate film, two cubes (1 mm × 1 mm) with a spacing of 1 mm were hollowed out. Next, Ag fabrics were used as flexible intercon-

nects, and TE legs were filled in the hollows with silver paste adhering the TE legs and Ag fabrics. Finally, a few drops of PDMS solution were added to encapsulate the device.



Scheme 2. Schematic illustration on integration steps of stretchable TEG.

2.5. Characterization

The microstructures of the hybrid films were observed by scanning electron microscopy (SEM, FEI Sirion 200). X-ray diffraction (XRD, Rigaku D/MAX 2200 PC with Cu-$K\alpha$ radiation $\lambda = 1.5406$ Å) and Raman spectroscopy (LabRAMHR800 using an Ar–Kr laser operating at 632.8 nm) were employed to analyze the phase and chain structures of the hybrid films. The electrical conductivity and Seebeck coefficient were measured using a ZEM-3 system (IULVAC-RIKO). Hall coefficients were measured using a Hall measurement system (Lakeshore 8400 Series, Model 8404) from room temperature to 200 °C.

2.6. Output performance measurement of TEG

To precisely control the temperature gradient applied across the TEG, a temperature control system has been setup as shown in Fig. S1. The TEG was placed on a temperature control stage (TLTP-FW-TEC2410D, Wuhan Talent Century Technology Co., Ltd.) maintained at a constant temperature, i.e., 25 °C as the cold end. A Peltier device, controlled by a DC power supply (TPR3005T-3C, Shenzhen Atten Technology Co., Ltd.) was employed as a heater to provide temperature at the hot end. Meanwhile, a thermometer (UT325, UNI-T Co., Ltd.) was used to monitor the temperature at the hot end. The output voltage of the TEG was recorded via a digit multimeter (Keithley, DMM 6500).

3. Results and discussion

3.1. Microstructures of Bi_2S_3@Bi/PANI hybrid films

The phases of the synthesized Bi_2S_3@Bi nanorods are checked by XRD as shown in Fig. 1(a). Since the positions of main diffraction peaks of Bi are very close to those of Bi_2S_3 (see the standard PDF cards), and peaks are overlapped due to the peak broadening, it could hardly differentiate Bi and Bi_2S_3 phases from these diffraction patterns. Instead, Bi_2S_3@Bi nanorods with different reduction reaction time are compared as shown in Fig. 1(b). Longer reaction time results in higher Bi content, thus, it could be identified from the increasing intensity of the peak assigned to the (012) plane of Bi that elemental Bi has been reduced and coexists with Bi_2S_3.

The microstructures of Bi_2S_3@Bi nanorods with different Bi contents in comparison with Bi_2S_3 nanorods (Fig. 2(a)) are shown in Figs. 2(b)–2(d). At low Bi content, i.e., with

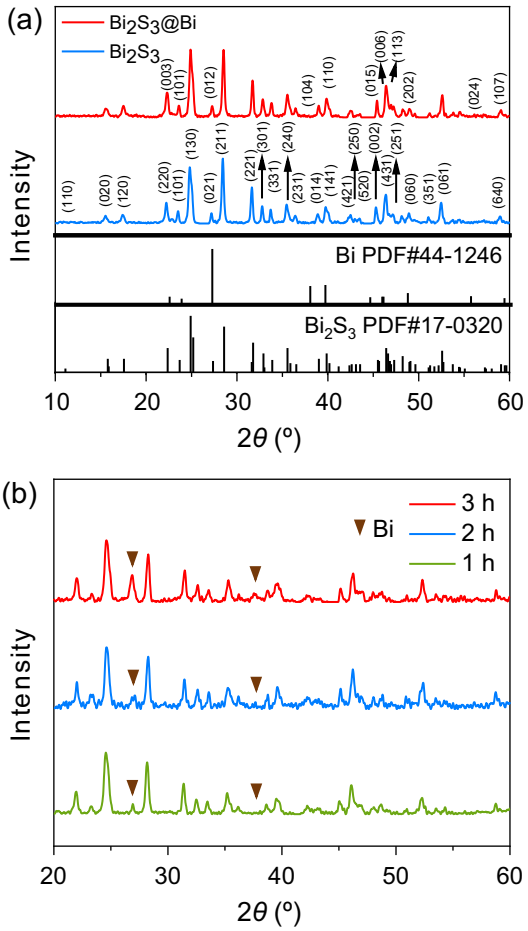


Fig. 1. (a) XRD patterns of Bi_2S_3@Bi core-shell nanorods in comparison with Bi_2S_3 nanorods. (b) XRD patterns of Bi_2S_3@Bi core-shell nanorods with different reduction reaction time.

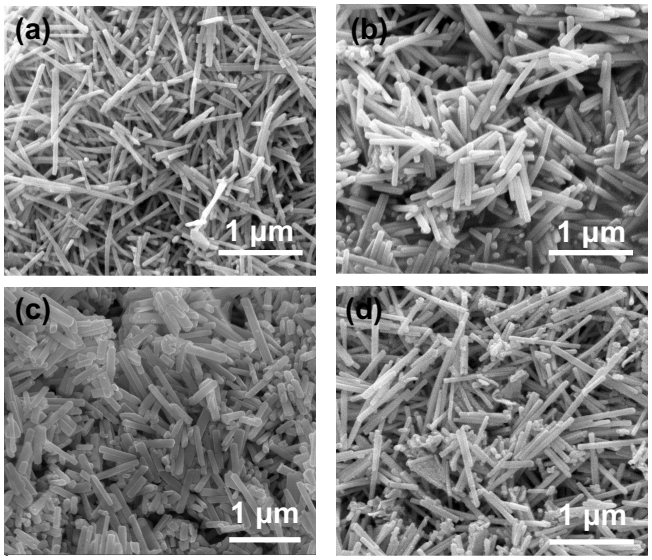


Fig. 2. SEM images of (a) Bi_2S_3 nanorods and Bi_2S_3@Bi core-shell nanorods with different reaction time: (b) 1 h, (c) 2 h, and (d) 3 h.

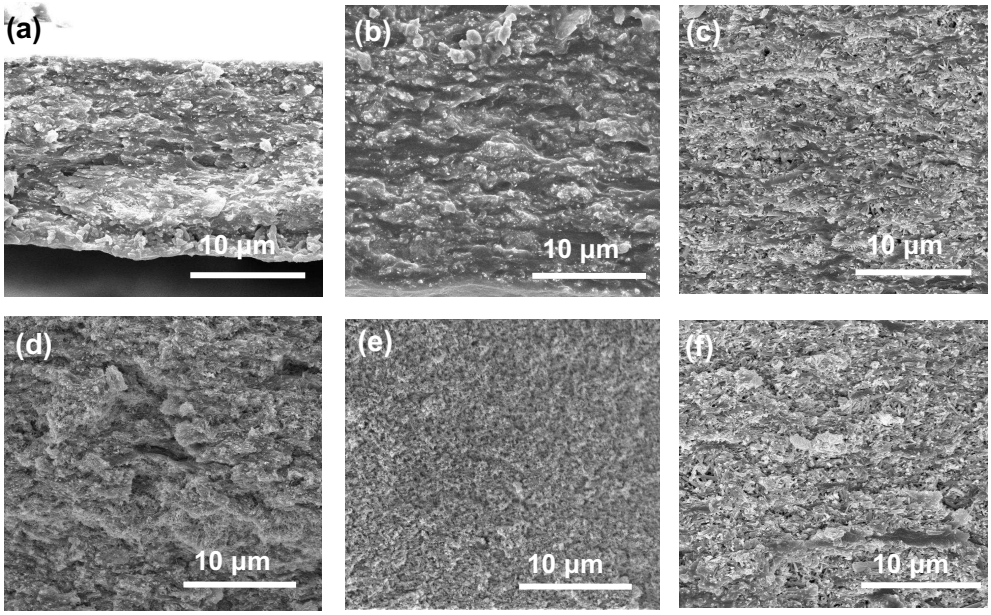


Fig. 3. Cross-sectional SEM images of Bi_2S_3@Bi/PANI hybrid films with filler content (a) 50%, (b) 60%, (c) 70%, (d) 80%, (e) 90%, (f) 70% hybrid film after heat treatment.

reaction time 1 h, the core-shell structure almost keeps the morphology of the Bi_2S_3 nanorod. As reduction reaction increases, the morphologies of some nanorods begin to collapse, resulting in shorter nanorods and a small number of nanoparticles (see Figs. 2(c) and 2(d)). Therefore, Bi_2S_3@Bi nanorods at reaction time 1 h were employed as fillers for hybrids.

Seen from the cross-sectional SEM images of the Bi_2S_3@Bi/PANI hybrid films shown in Figs. 3(a)–3(e) with filler loading increasing from 50% to 90%, the hybrid films present compact microstructure. The PANI turns into discontinuity as Bi_2S_3@Bi filler exceeds 70% weight fraction (see Fig. 3(c)), and the hybrid film becomes too fragile to be freestanding as Bi_2S_3@Bi loading reaches 90%. After heat treatment at 210 °C in vacuum, the interfaces between polymer and inorganic fillers become obscure (see Fig. 3(f)) compared to the morphology of the as-prepared film shown in Fig. 3(c), indicating slight change on polymer morphologies by heat treatment.

Further, Raman spectra were used to study the chemical bonds change brought by incorporation of Bi_2S_3@Bi fillers and heat treatment. As shown in Fig. 4, the typical vibrating modes of pure PANI occur at 1191 cm^{-1}, 1507 cm^{-1}, and 1563 cm^{-1} assigned to C–H bending vibration of the quinoid or benzenoid ring, N–H stretching vibration of the benzenoid ring, and C–C stretching vibration of the benzenoid ring, respectively.[21] Peaks at 1334 cm^{-1} are assigned to the C–N^+ vibration of the quinoid ring and 1403 cm^{-1} and 1638 cm^{-1} to the delocalized polarons in the expanded polymeric conformation. Incorporating Bi_2S_3@Bi generally reserves the expanded polymeric conformation as seen from the existence of the 1638 cm^{-1} mode in all the as-prepared hybrid films. Intensity increase of vibrating mode 1403 cm^{-1} is an indication that cross-linking of PANI polymer has occurred,[16] which becomes more intense in hybrids after heat treatment with Bi_2S_3@Bi loading exceeding 70%, in consistent with the microstructure change.

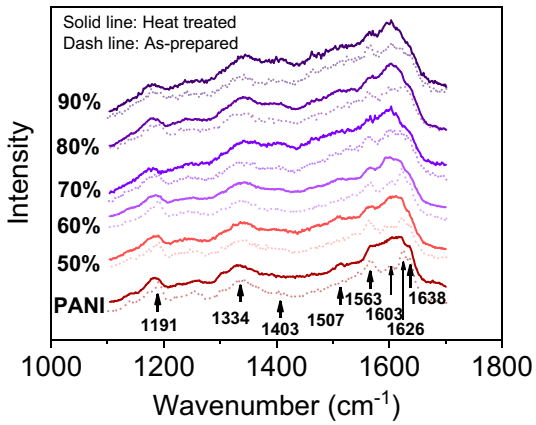


Fig. 4. Raman spectra of Bi_2S_3@Bi/PANI hybrid films with various Bi_2S_3@Bi contents before and after the heat treatment.

3.2. Thermoelectric properties of Bi_2S_3@Bi/PANI hybrid films

The temperature-dependent TE performances of the as-prepared hybrid films are shown in Figs. 5(a)–5(c). The electrical conductivity of the hybrid films, as shown in Fig. 5(a), decreases with increasing Bi_2S_3@Bi core-shell nanorods loading. This is due to their low electrical conductivity compared to PANI and the discontinuity of the conducting PANI polymer at high filler loading, which leads to sharp drop in the conductivity from 4700 S/m for 50% to 1057.8 S/m for 80% loading at room temperature. The significant decrease in the electrical conductivity of the hybrid films with increasing temperature is attributed to the decrease in crystallinity and loss of the emeraldine sequence due to chain scission, crosslinking of the PANI matrix as well as the partial loss of CSA. The

carrier in the as-prepared hybrid films at room temperature is still p-type, and due to the opposite carrier types of PANI and Bi_2S_3@Bi, the competition between carriers results in very low Seebeck coefficients as shown in Fig. 5(b), i.e., about 15 μV/K for 50% hybrid film and decreasing to 7.6 μV/K for 80% hybrid film. With increasing temperature to higher than 200 °C, a transition from p-type to n-type is observed, and the maximum Seebeck coefficient −150 μV/K is obtained in 80% hybrid film at 230 °C. Meanwhile, the power factor calculated for these Bi_2S_3@Bi/PANI hybrid films reaches the maximum value 5.24 μW/m·K^2 for 80% hybrid film at 230 °C shown in Fig. 5(c).

Temperature-dependent Hall effect measurement was carried out to study the transport behavior of the carriers of the Bi_2S_3@Bi/PANI hybrids. As shown in Fig. 5(d), the carrier concentration increases as the temperature rises, while the mobility decreases quickly, suggesting that the hopping of carriers in the polymer chains has been obstructed. As the temperature continues to increase exceeding 160 °C, the carrier concentration drops abruptly and the mobility turns its sign from positive to negative, originated from the change in Hall coefficient (R_H) according to $\mu = R_H/\rho$, where ρ is the resistivity. The observation thus reflects a change in major carrier from holes contributed from PANI to the electrons from Bi_2S_3@Bi, confirming that n-type material has been obtained at 200 °C.

To support the idea that Bi_2S_3@Bi core-shell heterostructure is more effective in enhancing the electrical conductivity of PANI-based hybrids so as to further optimize the n-type TE properties, TE properties of Bi_2S_3@Bi/PANI have been compared with those of Bi_2S_3/PANI hybrid films. As shown in Fig. 6, taking filler loading at 80% as an example, the as-prepared Bi_2S_3@Bi/PANI has higher electrical conductivity at room temperature (1057.8 S/m for Bi_2S_3@Bi filler vs. 718.6 S/m for Bi_2S_3 filler). Since Bi_2S_3@Bi filler could endure higher temperature up to 220 °C, the carrier concentration is adjusted to a more favorable value, thus the Seebeck coefficient continues to increase. PF is 5.24 μW/m·K^2 for Bi_2S_3@Bi/PANI and 0.97 μW/m·K^2 for Bi_2S_3/PANI, more than 4 times increment. It is worth noting that, Bi_2S_3@Bi heterostructure promotes not only electrical conductivity, but also leads to slightly higher Seebeck coefficient compared with Bi_2S_3, which probably comes from the energy filtering effect enabled by the Bi_2S_3/Bi/PANI multiple interfaces. The work function of Bi, Φ_{Bi}, is about 4.22 eV,[22,23] while the conduction band of Bi_2S_3 is around −4.27 eV,[24] the lowest unoccupied molecular orbital (LUMO) energy in PANI is −4.15 eV,[20] to equilibrate the Fermi levels, energy barriers would be formed at Bi_2S_3/Bi and Bi/PANI interfaces, permitting electrons with higher energy to pass through so as to give rise to the Seebeck coefficient of the Bi_2S_3@Bi/PANI hybrid film.

After the heat treatment, the room temperature TE properties of the hybrid films with different filler loadings are shown in Fig. 6(d). For all the hybrid films, the n-type is retained, and the higher content of Bi_2S_3@Bi filler, the higher Seebeck coefficient, showing a maximum value of −159.4 μV/K. However, due to the crosslink of polymer chains as well as the loss of partial dopant, the electrical conductivity is low. Finally, the optimal stable n-type Bi_2S_3@Bi/PANI has been obtained in 70% Bi_2S_3@Bi/PANI hybrid film with $PF = 0.246$ μW/m·K^2.

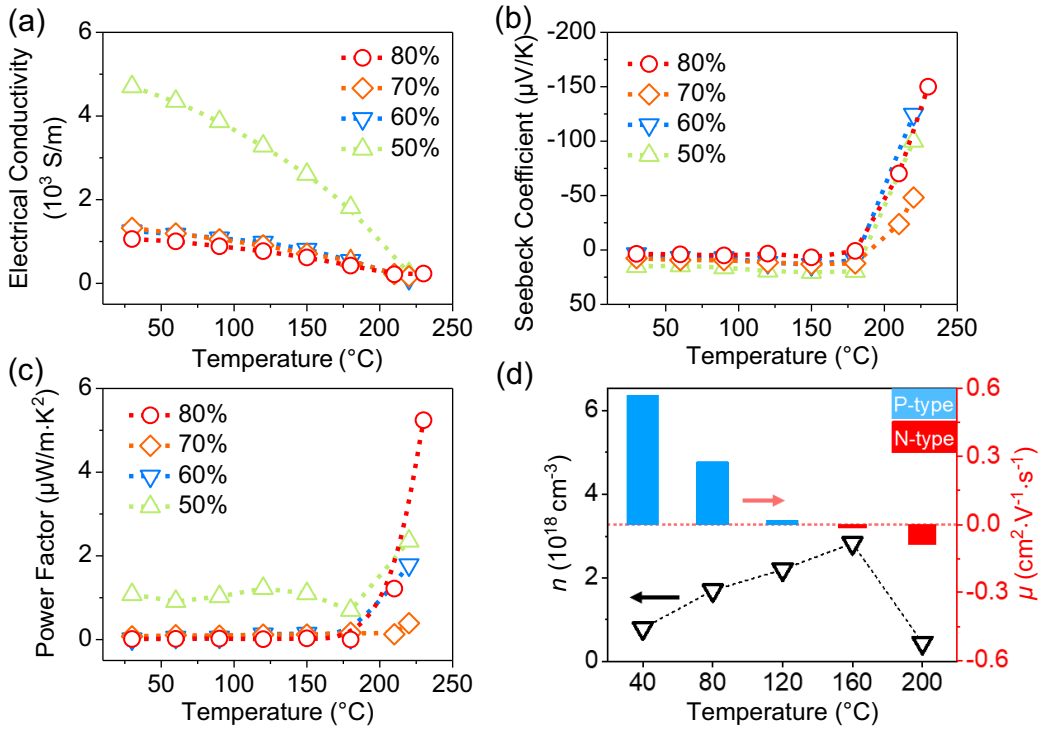


Fig. 5. Temperature-dependent thermoelectric properties of the as-prepared Bi_2S_3@Bi/PANI hybrid films: (a) electrical conductivity, (b) Seebeck coefficient, (c) power factor. (d) Temperature-dependent transport parameters, carrier concentration and mobility of Bi_2S_3@Bi/PANI film.

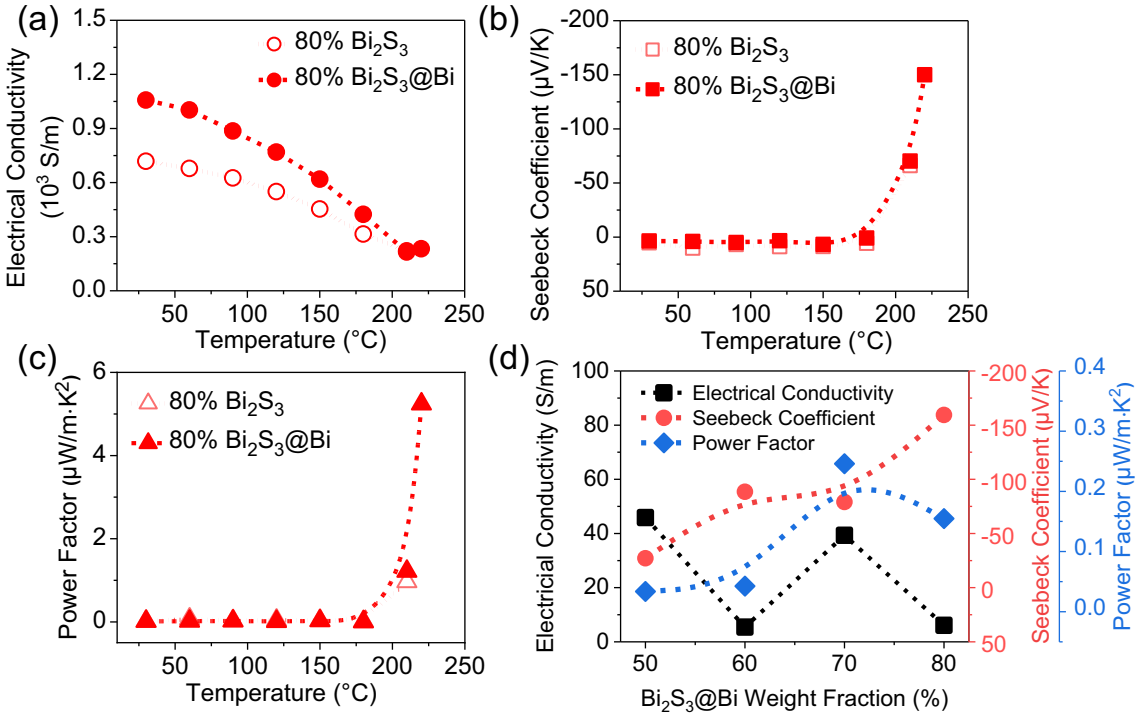


Fig. 6. Comparison on thermoelectric properties between Bi_2S_3@Bi/PANI and Bi_2S_3/PANI hybrid films at 80% filler loading. (a) Electrical conductivity, (b) Seebeck coefficient, (c) power factor. (d) Thermoelectric properties measured at room temperature of heat-treated Bi_2S_3@Bi/PANI films with different Bi_2S_3@Bi loadings.

3.3. Performances of stretchable TEG

The thermal energy harvesting functions of the integrated stretchable TEG from n-type Bi_2S_3@Bi/PANI and p-type Te-MWCNT/PANI hybrids are demonstrated in Fig. 7. Figure 7(a) presents the steady voltage responses to different ΔT. The output voltages with ΔT conform to a linear relationship, i.e., $V = |S| \times \Delta T$, where the slope is the sensitivity of the TE sensor. As shown in Fig. 7(b), the sensitivity of the as-fabricated device is about 84 ± 3 μV/K, and when placed in the atmosphere, the slope decreases about 15% to 71 ± 4 μV/K. The mechanical stability of the stretchable TEG was measured under a fixed temperature difference of 10 K with *in situ* external tensile strain loaded. As shown in Fig. 7(c), the output voltage decreases as the TEG elongation increases, due to increase in internal resistance from geometry variation and the gradually destruction at the joints where the electrodes interconnect the TE legs and encapsulated PDMS. The TEG could be stretched to 75% before broken, suggesting its good mechanical compliance.

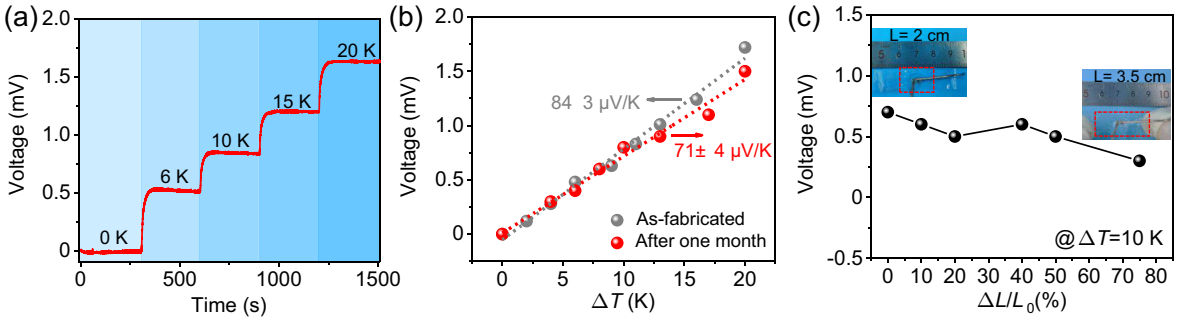


Fig. 7. (a) Steady responses of TEG to various temperature differences. (b) Comparison on the output voltages changing with ΔT of the as-fabricated TEG and stored one month later. (c) The *in situ* output performance measurement of the TEG with increasing stretching strain at a fixed temperature difference of 10 K.

4. Conclusion and perspectives

Core-shell heterostructured n-type Bi_2S_3@Bi nanorods have been incorporated into PANI to transform an intrinsic p-type polymer into n-type TE materials via carrier adjustment strategy in combination of a proper heat treatment processing. Heterostructured Bi_2S_3@Bi nanorods are more effective in improving the power factor of the hybrids than the Bi_2S_3 nanorods due to higher electrical conductivity brought by the Bi. Further, a pair of n/p bulk TE legs made from the PANI-based hybrids were integrated with elastomer substrate into stretchable TEG. Its function as thermal energy harvester showing stable output with thermopower 84 ± 3 μV/K for one

pair and little degradation over a one-month period in the air was demonstrated. The mechanical stability test showed that the TEG could withstand up to 75% elongation. This study has therefore provided a promising strategy to develop stretchable TEGs harvesting heat from environment with stable and high thermopower performances as long-term power supply.

Acknowledgments

The study was supported by the National Key Research and Development Program of China (Grant Nos. 2018YFA0702100 and 2018YFB0703600), the National Natural Science Foundation of China (Grant Nos. 51872009 and 92066203), Beijing Nova Programme Interdisciplinary Cooperation Project, and the Fundamental Research Funds for the Central Universities, China.

References

[1] Russ B, Glaudell A, Urban J J, Chabinyc M L and Segalman R A 2016 *Nat. Rev. Mater.* **1** 16050
[2] Bubnova O, Khan Z U, Malti A, Braun S, Fahlman M, Berggren M and Crispin X 2011 *Nat. Mater.* **10** 429
[3] Kim G H, Shao L, Zhang K and Pipe K P 2013 *Nat. Mater.* **12** 719
[4] Jiang F X, Xu J K, Lu B Y, Xie Y, Huang R J and Li L F 2008 *Chin. Phys. Lett.* **25** 2202
[5] Jacobs I E and Moule A J 2017 *Adv. Mater.* **29** 1703063
[6] Wan C L, Gu X K, Dang F, Itoh T, Wang Y F, Sasaki H, Kondo M, Koga K, Yabuki K Y, Snyder G J, Yang R G and Koumoto K 2015 *Nat. Mater.* **14** 622
[7] Wang L M, Zhang Z M, Liu Y C, Wang B R, Fang L, Qiu J J, Zhang K and Wang S R 2018 *Nat. Commun.* **9** 3817
[8] Wang M C and Lin S C 2016 *Adv. Funct. Mater.* **26** 5297
[9] Jin H L, Li J, Iocozzia J, Zeng X, Wei P C, Yang C, Nan L, Liu Z P, He J H, Zhu T J, Wang J C, Lin Z Q and Wang S 2019 *Angew. Chem. Int. Ed.* **58** 15206
[10] Wan C L, Tian R M, Kondou M, Yang R, Zong P G and Koumoto K 2017 *Nat. Commun.* **8** 1024
[11] Wu Z H, Xie H Q, Zhai Y B, Gan L H and Liu J 2015 *Chin. Phys. B* **24** 034402
[12] Xu Q, Qu S Y, Ming C, Qiu P F, Yao Q, Zhu C X, Wei T R, He J, Shi X and Chen L D 2020 *Energy Environ. Sci.* **13** 511
[13] Lu Y, Qiu Y, Cai K F, Ding Y F, Wang M D, Jiang C, Yao Q, Huang C J, Chen L D and He J Q 2020 *Energy Environ. Sci.* **13** 1240
[14] Ferhat M and Nagao J 2000 *J. Appl. Phys.* **88** 813
[15] Jiang C, Ding Y F, Cai K F, Tong L, Lu Y, Zhao W Y and Wei P 2020 *ACS Appl. Mater. Interfaces* **12** 9646
[16] Wang Y, Liu G F, Sheng M, Yu C and Deng Y 2019 *J. Mater. Chem. A* **7** 1718
[17] Biswas K, Zhao L D and Kanatzidis M G 2012 *Adv. Energy Mater.* **2** 634
[18] Ge Z H and Nolas G S 2014 *Cryst. Growth Des.* **14** 533
[19] Wang Y, Zhang S M and Deng Y 2016 *J. Mater. Chem. A* **4** 3554
[20] Wang Y, Yu C, Sheng M, Song S L and Deng Y 2018 *Adv. Mater. Interfaces* **5** 1701168
[21] Yao Q, Wang Q, Wang L M and Chen L D 2014 *Energy Environ. Sci.* **7** 3801
[22] Xiao J, Yang W Y and Li Q 2017 *Appl. Catal. B* **218** 111
[23] Jupnik H 1941 *Phys. Rev.* **60** 884
[24] Han D, Du M H, Dai C M, Sun D Y and Chen S Y 2017 *J. Mater. Chem. A* **5** 6200